

STATUS OF FAR-TECH'S ECR ION SOURCE OPTIMIZATION MODELING*

J. S. Kim[#], L. Zhao, B.P. Cluggish, I. N. Bogatu, S.A. Galkin, FAR-TECH, Inc. San Diego, CA
92121, U.S.A.

V. Tangri, Univ. Wisconsin, U.S.A.

R. Pardo, ANL, Argonne, IL 60439, U.S.A.

Abstract

FAR-TECH, Inc. has been building up a suite of comprehensive numerical tools for end-to-end Electron Cyclotron Resonance Ion Source (ECRIS) modeling. They consist of the Monte Carlo Beam Capture (MCBC) code [1, 2], the Generalized ECRIS Modeling (GEM) code [3], and the Ion Extraction (IonEx) code [4]. The MCBC code simulates beam slowing down dynamics in a plasma due to Coulomb collisions, and includes ionization due to hot electrons and charge exchange. GEM models ECR plasmas by fluid ions and bounce averaged electrons. MCBC provides ion source profiles to GEM, which in turn provides ion flux profiles to IonEx. IonEx accurately models the plasma meniscus formed during ion extraction using an innovative, meshfree, particle-in-cloud-of-points technique. Extensions of GEM to two dimensions (2D) and IonEx to three dimensions (3D), as well as experimental validation are underway.

INTRODUCTION

Electron cyclotron resonance ion sources are an efficient way to produce highly charged ions. High-charge-state ion beams and radioactive ion beams (RIB) are important for nuclear physics studies. In ECR “charge breeders” a beam of low (+1 or +2) charged ions is injected into an ECRIS plasma and charge bred to produce higher charge-state ions. Currently, charge breeders used for RIB productions are developed by trial and error. Future large, expensive ion sources will require modeling and diagnostics for optimal and efficient design. For this reason, FAR-TECH, Inc. has been developing an integrated suite of codes for end-to-end ECRIS modeling. It consists of three major codes; MCBC, GEM, and IonEx. This article gives a brief summary and status of the codes along with an example simulation.

MCBC MODELING BEAM DYNAMICS

MCBC is a Monte Carlo code which traces beam ion trajectories as test particles. Beam ions entering into a plasma experience drag by Coulomb collisions, a long range force. Ions of mass (m_s) and charge (q_s) observe the following equation of motion.

$$m_s \frac{d\vec{v}}{dt} = q_s \vec{E}(\vec{r}) + q_s \vec{v} \times \vec{B}(\vec{r}) + \text{Coulomb Collision}$$

We adapted Boozer’s formula [5,6] to treat the Coulomb collisions. Coulomb collisions are represented in two separate operations. The first is the scattering of the velocity vector of a test particle without changing its magnitude, and the second is the change in energy resulting from beam slowing down and energy diffusion.

The pitch-angle scattering operator relates the old (previous time step) velocity (v_{old}) and the new velocity (v_{new}) after a time step τ as follows:

$$\hat{v}_{new} = (1 - v_{\perp} \tau / 2) v_{old} \hat{v} + \sqrt{\left(1 - \frac{1}{4} v_{\perp} \tau\right) v_{\perp} \tau / 2} (\pm \hat{\phi} \pm \hat{\theta}) v_{old}$$

Here, the variables with hats are unit ortho-normal vectors in velocity space. The sign \pm refers to a random choice of signs in either direction on each time step. The angular scattering operator only changes the direction of ion velocity while conserving the ion energy. The new ion energy (E_{new}) is calculated with the energy scattering operator,

$$E_{new} = E_{old} - \frac{2v_s \tau}{1 + m_i / m_b} \left[E_{old} - \left(\frac{3}{2} + \frac{d \ln v_s}{d \ln E_{old}} \right) T_i \right] \pm 2 \sqrt{\frac{T_i E_{old} v_s \tau}{1 + m_i / m_b}}$$

where E_{old} is the old (previous time step) ion energy.

The first term describes the slowing of the ion and the second term describes the diffusion of the beam energy, where the \pm symbol refers to a random choice of sign taken on each time step. The magnitude of the new velocity vector is determined by this new energy. Combining the two steps, the new velocity after Coulomb collisions is obtained. Note that the mass dependence in the equation, which does not appear in Boozer’s formula, was added to properly represent the different masses of beam ions and the plasma ions. Other collisions such as ionization and charge exchange are treated by a rejection method [1, 7]

GEM MODELING ECRIS PLASMA

GEM was written to use experimental ‘knobs’ to model ECRIS plasmas [3]. It has fluid ions, bounce averaged Fokker-Planck electrons, and flux conserving neutral models. The Fokker-Planck equation is solved to obtain the non-Maxwellian electron energy distribution function

*Work supported by US DOE SBIR program
#kim@far-tech.com

[8]. Using experimental ‘knob’ inputs, GEM predicts the ion Charge State Distribution (CSD) and charge breeding times. Extension to 2D GEM is underway [9].

ECR CHARGE BREEDER SIMULATION

First, the plasma parameter profiles are obtained by running the time-dependent GEM simulation until a steady state is achieved, using experimental parameters as an input. Figure 1 shows the results of a simulation of the Argonne ECR-I device with an oxygen plasma. The peak electron density is $7 \times 10^{11} \text{ cm}^{-3}$. The plasma column extends from $z=19\text{cm}$ to $z=48 \text{ cm}$. The peak magnetic field is 1.4 T. While GEM can find the self consistent electrostatic field in an ECRIS, for purposes of this presentation, we assumed $E=0$ everywhere. Its effect is described in the simulation discussion.

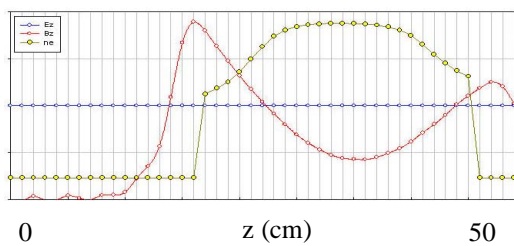


Figure 1: Electric field (blue), magnetic field (red), and electron density profile (yellow with circles).

Next we trace beam ions entering the plasma by MCBC. At entry the beam radius is 1mm, and the ions are injected all together at once. Snapshots of captured ions, slowed down to that of plasma ion thermal energy, are shown in Fig. 2 at $10 \mu\text{s}$ (left figures) and $30 \mu\text{s}$ (right figures) for 5eV and 15 eV Ar $1+$ beams. The bottom row figures are with no magnetic fields.

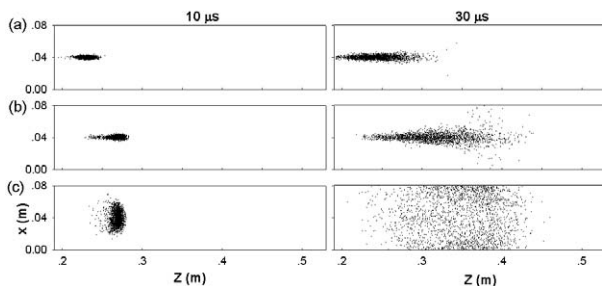


Figure 2: Snapshots of captured ions $10 \mu\text{s}$ (left figures) and $30 \mu\text{s}$ (right) after the ions enter the device at $z=0.19 \text{ m}$. (a) Beam energy of 5 eV (b) Beam energy of 15 eV (c) Beam energy of 15 eV, no magnetic field.

The magnetic field confines the ions by guiding the ions flow along the field lines. This improves the capture efficiency because the ions are not lost to the radial wall, resulting in a higher CSD.

Thermalized ions may be treated as sources to the background plasma. Captured ion profiles for beam energies of 5, 15 and 30 eV are shown in Figure 3.

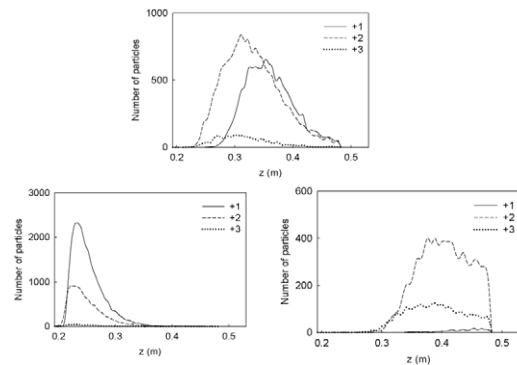


Figure 3: Captured ion profiles for three different energies of the injected ion beam; 5 eV (bottom left), 15 eV (top), and 30 eV (bottom right).

Charge breeding times can be evaluated from the time evolution of CSDs (See Fig.4). The values are similar to experimentally observed values [10].

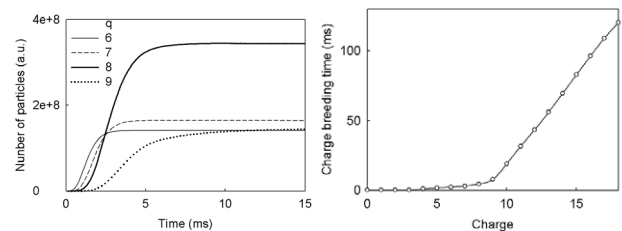


Figure 4: (Left) Time evolution of Argon charge states of 6+, 7+, 8+, and 9+, modeled by GEM. The GEM input is the captured ion profile from MCBC using a 15 eV injected Ar $+$ beam. (Right) Argon charge breeding time as a function of charge state.

The steady state charge breeding efficiencies for different charges states of argon are shown in Fig. 5 for injected beam energies of 5, 15, and 30 eV. These were obtained by running the GEM simulation a second time, using the ion profiles shown in Fig. 3 as additional input sources, to obtain a new steady state and CSD. A high beam energy was most efficient for producing low charge state ions and vice versa. The reason for this is that high energy ions penetrate deeply into the plasma and are captured close to the extraction aperture or even pass right through the plasma, so that few of the low charge state injected ions are lost to backstreaming but their residence time for charge breeding is short. Low energy ions are captured close to the injection aperture and suffer large losses to backstreaming, but the few ions that do stay in the plasma have a long residence time and become highly charged before leaving through the extraction aperture.

Note that we define the extraction current here as the ion flux integrated over the plasma cross section at the extraction end of the device. However, the area of the extraction aperture in an ECR charge breeder is typically much smaller than the cross-sectional area of the plasma, which would reduce the efficiencies shown here by the ratio of areas.

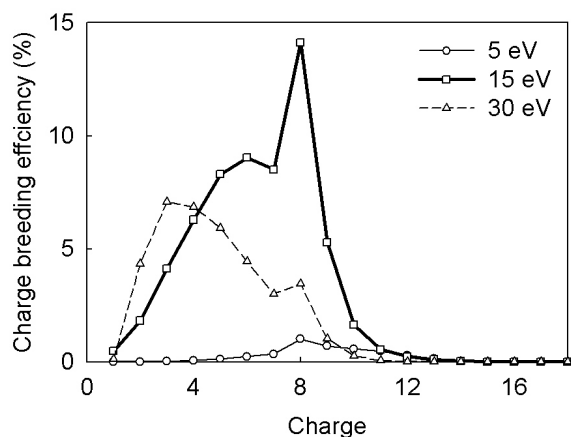


Figure 5: Steady state argon charge state distributions for three different energies (5, 15, and 30 eV) of the injected ion beam.

Discussion of Simulation Results

The results of our charge breeding simulations are summarized in Table 1. The first three rows show the results of the MCBC calculations for three beam energies. For 5 and 15 eV the vast majority of ions are captured (f_{capt}), whereas for 30 eV a significant fraction of ions are lost to the walls (f_{lost}) or pass through the device (f_{pass}). The next row shows the fraction of ions extracted from the device (assuming the extraction aperture is the same radius as the plasma) by GEM. The extracted fraction, including both ions that are captured and then extracted as well as ions that pass through the device, is given by

$$f_{extract} = \frac{f_{pass}I_{in} + \sum I_n / n}{I_{in}}$$

where I_{in} is the current of the singly charged input ion beam, and I_n is the output current of ions of charge state n .

Table 1: Summary of charge breeding results

Beam Energy:	5 eV	15 eV	30 eV
f_{capt}	100%	98%	55%
f_{lost}	0%	2%	13%
f_{pass}	0%	0%	32%
$f_{extract}$	4%	41%	81%
q (efficiency of max CSD)	3+ (8%), 4+ (8%)	+8 (12%)	+10 (1%)

Note that despite the low capture efficiency for the 30 eV, the extracted particle flux is larger than that at 15 eV, due to the large fraction of ions which pass through the device. The charge state and efficiency of the maximum CSD are shown in the bottom of the table for three input beam energies. The extraction efficiency for Ar+8 ions at 15 eV is larger than the extraction efficiency for any charge state at either 5 or 30 eV, the 15 eV beam energy.

Thus 15 eV is optimum beam energy for production of a mono-charged extracted beam. This result points to the importance of tuning the beam energy so that the ions are captured in the center of the device.

The simulation presented assumed no electrostatic fields in the plasma. With plasma sheath potential, the optimum beam energy is higher by the sheath potential. The central ion confining electrostatic fields will be included in the future simulations.

IONEX MODELING PLASMA MENISCUS

IonEx is being developed with an innovative method to resolve the plasma meniscus accurately. As the region of meniscus is orders of magnitude smaller than the plasma dimensions, IonEx utilizes an adaptive meshfree technique. The 2D version is well benchmarked with IGUN [11], and 3D extension is underway.

SUMMARY OF STATUS

We are currently upgrading the GEM and MCBC codes in order to improve their accuracy. These upgrades include converting GEM from 1D to 2D by adding the radial dimension and including the plasma electric fields in the calculation. We are also extending IonEx to 3D to model the effect of the shape of the plasma sheath (plasma meniscus) on the injected and extracted ion beams. The three codes should provide end-to-end ECR plasma simulation. Validation of the codes is underway.

REFERENCES

- [1] J.S. Kim, C. Liu, D.H. Edgell, and R. Pardo, Rev. Sci. Instrum., 77, 03B106 (2006).
- [2] J.S. Kim, L. Zhao, B.P. Cluggish, and R. Pardo, Submitted to Rev. Sci. Instrum for publication.
- [3] D.H. Edgell, J.S. Kim, and I.N. Bogatu, R.C. Pardo and R.C. Vondrasek, Rev. Sci. Instrum., 73, 641 (2002).
- [4] S. A. Galkin, B. P. Cluggish, J. S. Kim, and S. Y. Medvedev, to be published in Proc. Pulsed Power and Plasma Science Conference 2007. Section 8B6, Albuquerque 17-22 June, 2007.
- [5] A.H. Boozer and G. Kuo-Petravic, Phys. Fluids 24, 851 (1981)
- [6] A. H. Boozer, Phys. Plasmas 9, 4389 (2002)
- [7] C.K. Birdsall, IEEE trans. Plasma Sci, 19, 65 (1991)
- [8] A. Mirin, M. McCoy, G. Tomaschke and J. Killeen, Comput. Phys. Commun. 81, 403 (1994)
- [9] L. Zhao, J.S. Kim, B.P. Cluggish, This proceeding, TUPAS079
- [10] F. Ames, R. Baartman, P. Bricault, K. Jayamanna, M. McDonald, M. Olivo, P. Schmor, D.H.L. Yuan, and T. Lamy, Rev. Sci. Instrum., 77, 3B03 (2006).
- [11] R. Becker and W. B. Hermannsfeldt, Rev. Sci. Instrum., 63 (4), 2756 (1992)